ORIGINAL PAPER

Flow characterization in T-shaped and cross-shaped micromixers

**Nassim Ait Mouheb · Agnes Montillet · Camille Solliec ·
Jaromir Havlica · Patrick Legentilhomme · Jacques Comiti ·
Jaroslav Tihon**

Abstract The understanding of physical phenomena such as flow behaviour and mass transfer performance is needed in order to develop appropriate micromixers for industrial or biomedical applications. In this article, the flow behaviour of the T-shaped and the cross-shaped micromixers with square cross-section are studied through numerical and experimental investigations. The comparisons are based on identical treated fluxes. From the particle image velocimetry (PIV) measurements, the flow topologies in the T-shaped and cross-shaped micromixers are very different. After liquid impact, it is observed that the vortex structures cover a longer part of the outlet channel in the case of the cross geometry. This result indicates that the cross-shaped micromixer could improve the mixing process in comparison with the micromixers having T geometry. A second experimental technique has been used, the electrochemical one, involving microelectrodes placed at several wall positions of the cross-shaped micromixer. The electrochemical method can locally characterize the formation of swirling flows. The high values of wall shear rate, in the impact zone, confirm the near wall disturbance created by the impingement of the flow and also the appearance of vortices that could enhance fluid mixing.

N. Ait Mouheb · C. Solliec
GEPEA UMR-CNRS 6144, Ecole des Mines de Nantes,
BP 20722, 4 Rue Alfred Kastler, 44307 Nantes, France

A. Montillet (✉) · P. Legentilhomme · J. Comiti
GEPEA UMR-CNRS 6144, C.R.T.T, 37 Bd de l'Université,
BP 406, 44602 Saint-Nazaire-Cedex, France
e-mail: agnes.montillet@univ-nantes.fr

J. Havlica · J. Tihon
Institute of Chemical Process Fundamentals, A.S.C.R,
Rozvojová 135, 16502 Prague 6, Czech Republic

1 Introduction

In the objective of building factories that are cleaner, safer, more efficient and better integrated into the landscape, many parameters constrain today's academic and industrial researchers to rethink process engineering. Thus, microfluidics appears as one of the most dynamic emerging aspects in such domains as microtechnology, analytical sciences or biotechnology. The main advantages of microprocesses consists in highly efficient micromixing, high surface-to-volume ratios, efficient heat transfer ability, avoidance of hot spots by effective temperature control and high operational safety (Kockmann 2008).

The mixing process is fundamental in many unit operations and forms the basic operations in other processes like heat exchangers or chemical reactors. The understanding of physical phenomena, such as flow behaviour and mass transfer performance is needed in order to develop these microprocesses for various applications. In the case of microchannels applied in combination with low processing flow rate, the small physical dimensions imply low Reynolds numbers (Re), typically ranged between ~ 0.1 and 1,000 (Wong et al. 2004; Mansur et al. 2008), and laminar flow. As a consequence of low Reynolds numbers, mixing in microchannels relies on molecular diffusion which is very slow compared to convection. The critical dimensions that govern the extent of diffusion are the diffusion distance and the residence time between species along the channel. These mass transfer parameters can be optimized, based on the effect of the flow direction changes used for mixing intensification (bend, narrowing,

impingement,…) when mixing is not possible by turbulent flow generation (Hessel et al. 2003; Mansur et al. 2008).

In order to enhance mass transfer in the micromixers, many studies have been done concerning different geometries and flow configurations. Indeed, intensification of mass transfer within passive micromixers mainly depends on the flow topology after the fluid impact. In this study, we characterize the flow regimes along T and cross-shaped micromixers using numerical and experimental methods.

Our first attention in the study of a T-shaped micromixer is to validate the protocols implemented in numerical simulations and experimental methods by comparing our results from various studies available in the literature. The study of liquid mixing in T-shaped micromixers was previously carried out by several authors such as Engler et al. (2004), Ait Mouheb et al. (2008) and Soleymani et al. (2008). They highlighted three laminar flow regimes in the mixing channel: stratified flow, vortex flow and engulfment flow. According to Soleymani et al. (2008), the Reynolds numbers of transition between successive regimes depend on the aspect ratio between the height and width of channel. At very low aspect ratio, the flow inside the mixing channel flows in the stratified regime due to the high wall friction of the fluid, which results in high values of pressure drop. By increasing the aspect ratio, the pressure drop decreases and changes in the flow patterns are observed namely, a transition from stratified flow to vortex flow and then to engulfment flow.

The second geometry, the cross-shaped one, can be regarded as a recent approach that has not been completely studied in the scope of micromixer designing. The flow patterns observed in these systems interest us because the fluid converges in an impact area giving rise to strong shear and therefore intensifies mass transfer. Srisamran and Devahastin (2006) studied numerically a cell with two microchannels crossing at right angles. With the increase of the Reynolds number, the numerical simulations show the appearance of recirculation zones. The diameter of these vortices increases with an increase in the Reynolds number. The appearance of recirculation zones and preferential zones in the case of crossing microchannels was confirmed by the experimental work using an electrochemical method and the numerical studies performed by Huchet et al. (2008) with microchannels 500 and 833 µm, respectively, in hydraulic diameter. Values of the mean shear rate were determined from electrochemical measurements; they reveal the existence of high hydrodynamic instabilities and three-dimensional flow in the outlet channels which improve mixing processes.

In our study, the characterization of the flow in T-shaped and cross-shaped micromixers is based on the use of several complementary methods of investigation, whether numerical or experimental, which can thus lead to comprehensive and complementary information. The experimental study is made by the Particle Image Velocimetry (PIV) and electrochemical methods. Two cells are constructed, for both geometries (T-shaped and cross-shaped) using square channels with 400 µm hydraulic diameter. In order to use particle image velocimetry (PIV), a system is adapted so as to measure the velocity fields in various channel planes, at different channel depths. This allows the observation of the flow evolution and the vortices development along the microchannels. A second experimental technique, the electrochemical one, is used; it involves microelectrodes placed at several positions on the channel wall and located near the crossing. The electrochemical wall microprobes are often used to obtain local wall shear rate (Mitchell and Hanratty 1966). Presently, this non-intrusive method is used inside a cross-shaped micromixer. These two complementary experimental data will be analysed and compared with the CFD results.

2 Materials and experimental method

2.1 Flow pattern characterization using an adapted particle image velocimetry

In order to characterize flow patterns, the measurement of the velocity distribution inside the liquid is performed using particle image velocimetry (PIV) with appropriate resolution. The adapted PIV system used in this study is presented in Fig. 1. Polyamide seeding microparticles of 5 µm average diameter and characterized by a density equal to 1,030 kg m^{-3} (Dantec dynamic®) are added to the liquid. These particles are illumined by a pulsed Nd:YAG laser NewWave® Solo at a wavelength of 532 nm. Pairs of two images are successively captured with a CCD camera having a 1,600 × 1,186 pixels resolution.

For the microfluidic measurements, a zoom system '12 × Zoom Lens System LaVision' is adapted to our camera. The optical set-up (Fig. 1) allows changing the spatial resolution from 4.8 mm × 6.4 mm for the lowest magnification to 0.2 mm × 0.4 mm for the maximum magnification. The depth of field in the microchannels is approximately equal to 30 µm. This depth is equivalent to 1/13 of the channel width, based upon the size of the first interrogation window and the measurement depth of the zoom lens.

The motion of the fluid is determined by measuring the displacement of seeding particles in two recorded images separated by a known period of time. Each image is divided into a given number of cells, named interrogation areas, each of these containing a minimum amount of particles. The measurements are analyzed using a standard cross-correlation routine (FlowManager, Dantec®) to yield the instantaneous velocity vector field.
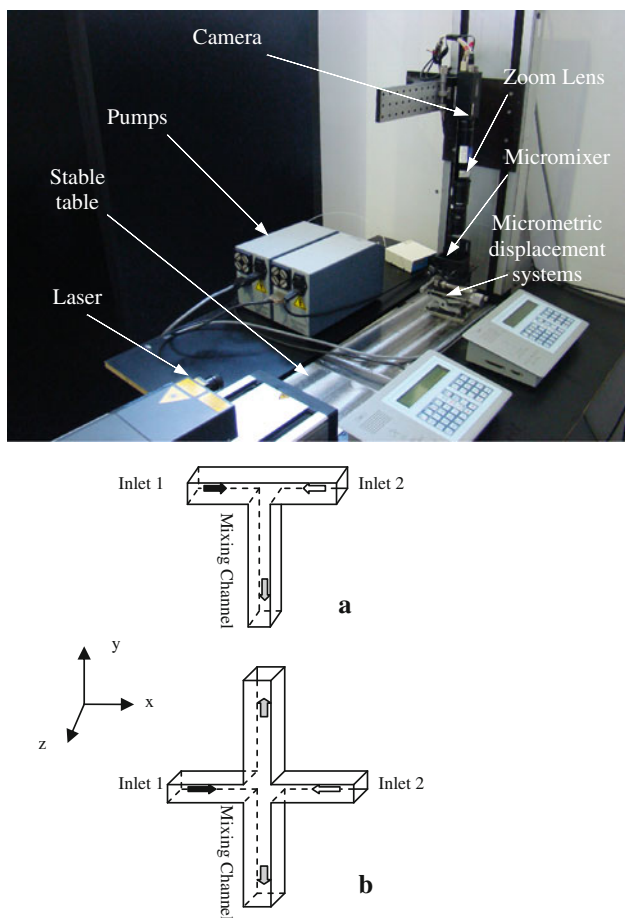
Fig. 1 PIV setup and schematic representation of **a** T-shaped and **b** cross-shaped micromixers

For PIV study, the micromixers were fabricated by milling PMMA. This device consists of two layers: a bottom PMMA layer including the channel structures with T and cross geometries, and a top PMMA layer for optical access with fluidic connections. The microchannels have a square cross-section of 400 μm in side. According to Soleymani et al. (2008), the development of vortices and the increasing of the mass transfer are amplified with the height of the channel until an optimal value is reached. In our study, the choice of square-sectioned channels and a hydraulic diameter equal to 400 μm are due to technological constraints such as milling microchannels in PMMA and building a system equipped with micro-electrodes (Sect. 2.2.3). Consequently, the mean fluid velocity in the mixing channel is twice more important that the inlet velocity in the T-shaped micromixer. In the cross geometry, the mean fluid velocity is the same in the inlet channels and in the outlet channels. This difference will be taken into account in the flow regimes characterization.

The micromixers are placed on a micrometer displacement system. This system allows to move the studied system in two directions (horizontal and vertical) as well as

to rotate it. Thus, the velocity data are recorded for various channel planes at different channel depths within the microsystems. The system of vertical displacement is also used to position the illumination plane.

2.2 Electrochemical method

2.2.1 Principle

The electrochemical technique presented in this study is usually implemented to measure the mass transfer coefficient at working electrode surfaces. A potential difference is applied between an anode and a cathode or so-called 'working electrode' (Fig. 2). Small probes are flush-mounted in the wall; they allow to measure local values of wall shear rate (Hanratty and Campbell 1983). The probe active surface works as a small electrode where a fast electrochemical reaction takes place. The reduction of ferricyanide ions on the cathode is the most popular electrochemical reaction used for such flow diagnostics:

$$Fe(CN)_6^{-3} + e^- \rightarrow Fe(CN)_6^{-4} \tag{1}$$
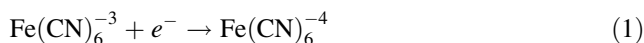
The measured intensity increases with the potential difference applied between the anode and the cathode until reaching a constant value, I_{lim}, corresponding to the diffusion limiting conditions. The current is then measured under diffusional limiting conditions such that the reaction rate is diffusion-controlled through the mass transfer boundary layer, δ_d. The ionic migration is negligible due to the presence of a supporting electrolyte. The limiting diffusion current can be linked to the mass transfer coefficient, k, the bulk concentration of the reacting species, c_0 and the surface of the electrode, A:
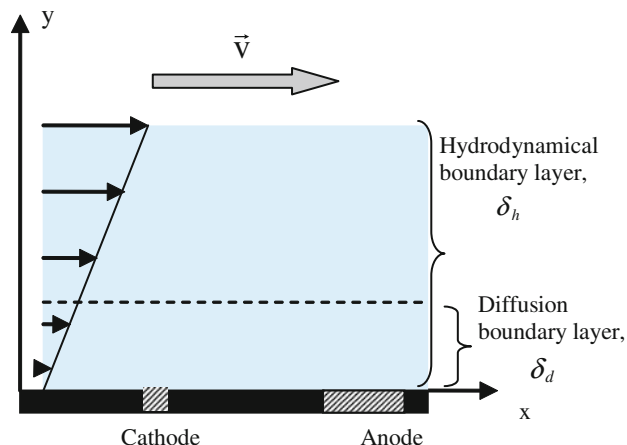
$$k = I_{lim}/v_e F A c_0 \tag{2}$$

Fig. 2 Electrochemical method principle

where v_e is the number of electrons involved in the electrochemical reaction, F is the Faraday's constant ($F = 96,500$ Cb mol^{-1}).

The mean measured limiting current, I_{lim}, is controlled by convective diffusion. The Lévêque's formula is applied to determine the mean wall shear rate S_y (Lévêque 1928).

$$I_{lim} = 0.8075 v_e F c_0 A (S_y D^2/l_e)^{1/3} \qquad (3)$$

where l_e is the width of electrode and D is the diffusivity of the ferricyanide ions in the solution.

2.2.2 Electrochemical experimental set-up

Figure 3 illustrates the experimental set-up used to measure the wall shear rate along the cross-shaped micromixer. The measurement set-up includes a micromixer fitted with microelectrodes, connected to the amplification and electrochemical signal acquisition system.

The circulating solution (potassium ferricyanide 0.01 M, potassium ferrocyanide 0.025 M, potassium sulphate 0.6 M) is kept at constant temperature (22°C). The density and the dynamic viscosity of this solution are equal to 998.2 kg m^{-3} and 1,003 Pa.s, respectively. The measurements of the diffusion coefficient, D, of the ferricyanide ions inside the working solution were obtained by the Levich method (Levich 1962) which uses a rotating disc electrode system; the value obtained at 22°C is 5.81×10^{-10} m^2 s^{-1}. A polarization voltage of -0.7 V is applied to ensure limiting diffusion current conditions at the electrodes. The measured current signals from the electrodes are converted into voltage signals, amplified and recorded by a PC computer. Current signals are measured at a 6 kHz sampling frequency during 90 s.

The PIV and electrochemical solutions are primed into the microsystem by using two micro annular gear pumps
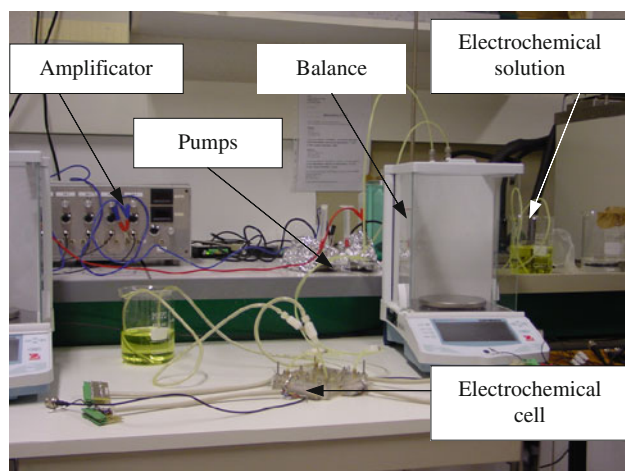

Fig. 3 Electrochemical experimental set-up

HNP Mikrosysteme GmbH® (mzr-4608) and the two inlet flow rates are adjusted to the same value. Simultaneously, the mass flow rates at the two outlets of the cross-shaped micromixer are measured at the same acquisition frequency by using two Ohaus explorer pro-balances (accuracy of 1 mg).

In order to limit the external electrical noises inherent to the recording of low amplitude currents, the following precautions were taken: (i) the measuring cell is introduced into a Faraday box, (ii) electrical cables and pumps are electrically insulated.

2.2.3 Electrochemical cell fabrication

For the electrochemical method, the experimental plates presented in Fig. 4 were realized at the Institute of Chemical Technology of Prague. They featured two crossing microchannels intersecting at right angle (cross geometry).

The microsystem consists of three main parts: (i) a PMMA bottom plate including the cross-shaped geometry, (ii) a PMMA upper plate with gold micro-electrodes and (iii) the electrical and hydraulic connections. The micromixer geometry is made by mechanical milling of PMMA. Gold electrodes are managed by a novel technique based on sacrificed substrate. The steps of the technique are as follows: (i) UV lithography on a metallic substrate (Fig. 5a, b), (ii) filling the structures in the photoresist with gold (galvanic deposition) (Fig. 5c), (iii) photoresist stripping (Fig. 5d), (iv) embedding gold structures in UV curable resin Acri-fix® 192 (Degussa) (Fig. 5e) and (v) metallic substrate removal (Fig. 5f).

The bonding process was to press together the individually structured PMMA plates and to subject them to a temperature of 126°C in an electrically heated vacuum oven for 12 min. Electrical connections are then fixed on the plates with an UV curable polymer resin. Alignment of the embedded electrodes with fluidic structures was done under microscope. Such metal structures are characterized by a high mechanical stability due to a thickness of 4–7 μm of gold structures built-in the curable resin. More details about the fabrication are provided in Schrott et al. (2009).

The electrochemical cell channels represented in Fig. 4 have a square section of 400 μm in sides. Rectangular microelectrodes made of a thin gold layer are included in the upper wall of the flow cells; they do not exceed the wall surface of the channel. Their width is 50 μm and their length is 400 μm.

The electrochemical cell contains 11 microelectrodes per channel; they are located at the same positions in each channel. Because of this symmetry, in the frame of our study, 16 electrodes have been used to investigate the flow structure. Eight microelectrodes (I1–I8) are located in an
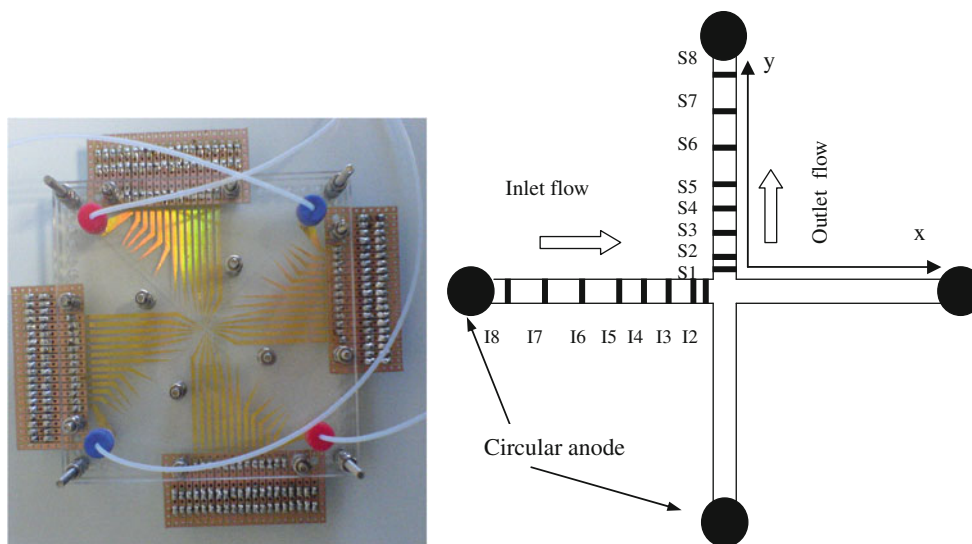
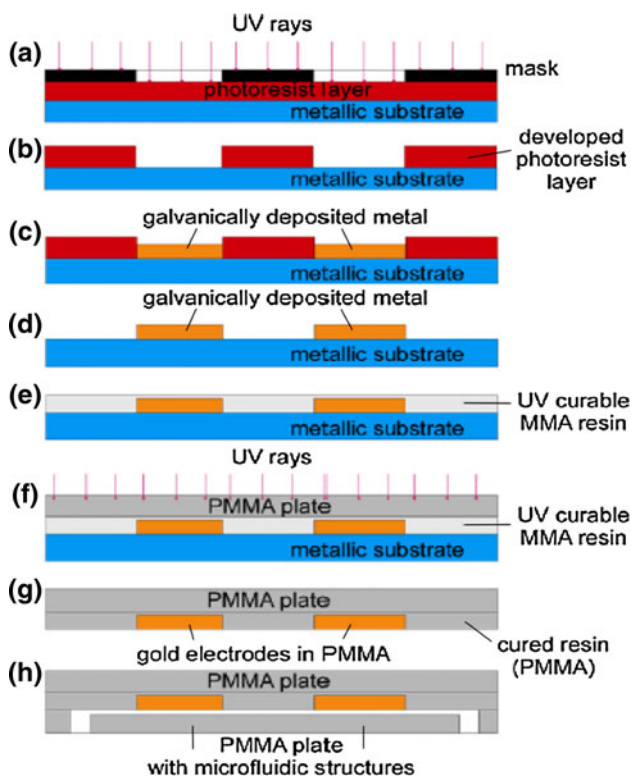**Fig. 4** The electrochemical cell and scheme of probes positions

Fig. 5 Fabrication Principle of the electrochemical cell (Schrott et al. 2009)

inlet channel and eight other microelectrodes (S1–S8) are located in the mixing channel. The microprobes, designated as S1 and S3, are located just after the crossing junction in order to get information on the disturbance provided by the crossing. The other probes are expected to provide data on the establishment length of the flow in the

outlet channel. The information about the positions of the different probes (Fig. 4) is provided in Table 1.

3 Computational procedure

The simulations were carried out in the respective configurations of the T-shaped and cross-shaped micromixers. The T-shaped micromixer (Fig. 1a) includes three channels: namely Inlet 1, Inlet 2 and a mixing outlet channel, whereas in the case of the cross-shaped micromixer (Fig. 1b) there are two input channels and two mixing outlet channels. The dimensions of the inlet channels are 16 mm (length) $\times$ 400 µm (width) $\times$ 400 µm (height) and those of the mixing channels are 24 mm (length) $\times$ 400 µm (width) $\times$ 400 µm (height).

The intersection between these channels is defined as the impact zone. A three-dimensional Cartesian coordinate system with y-axis pointing away from the observer is chosen for the calculations (Fig. 1a, b). The origin of the axis (0, 0, 0) is set in the centre of this impact zone. The computations are performed with hexahedral grids elements. The influence of the size of the mesh was tested in order to choose the appropriate grid for computation. The velocity profile was calculated at Re = 50 in a cross-section located at $x = 2D_h$ and with three different grids, respectively: 100×100 (grid a), 200×200 (grid b) and 400×400 (grid c). As the difference between the results obtained from grids b and c was less than 1%, grid b was selected for the computation.

A uniform velocity profile is assumed at the entrance of the inlet channels. The length of the inlet channels (16 mm) corresponds to $40D_h$; it is selected in order to

Table 1 Positions of the microprobes in the mixing channel

Microprobes	S1	S2	S3	S4	S5	S6	S7	S8
y, position in the channel (mm)	0.4	0.6	1.0	1.8	4.2	12.2	25.2	33.5
Corresponding number of D_h	D_h	$1.5D_h$	$2.5D_h$	$4.5D_h$	$10.5D_h$	$30.5D_h$	$63D_h$	$83.7D_h$

ensure a fully developed flow before the fluid impingement. For the calculations, the pressure at the exit is assumed to be the local atmospheric pressure. No-slip boundary condition at the side walls is applied. In order to facilitate comparisons of the flow behaviour as a function of the Reynolds number, the inlet velocities are set accordingly.

Considering the perspective of micromixer applications in the industrial production, we compare the performance of the two studied systems based on a given treated flux. Then, the Reynolds number is calculated using the inlet velocity as:

$$Re = \frac{\rho U D_h}{\mu} \tag{4}$$

where ρ and μ are the density and the dynamic viscosity of the fluid, respectively. They are equal to 998.2 kg m^{-3} and 1,003 Pa.s, respectively. U is inlet velocity and D_h hydraulic diameter of channel.

The solution of the problem described by the Navier–Stokes equations uses the finite volume method, implemented in the commercial CFD code FLUENT^{TM} 6.2 (Fluent Inc., Lebanon, NH). The integration of the discrete equations coupled in pressure/velocity formulation is realized by the implicit algorithm SIMPLEC (Fluent User Guide). The fluids are assumed to be incompressible and Newtonian. The flow is not affected by gravity and, to solve the following equations, it is considered as steady state and laminar:

$$\nabla \vec{v} = 0 \tag{5}$$

$$\nabla (\rho \vec{v} \otimes \vec{v}) = -\nabla p + \nabla [\mu (\nabla \vec{v} + \nabla \vec{v}^T] \tag{6}$$

Here, p is pressure in micromixer and $\vec{v}$ velocity vector.

In the present study, the numerical simulation of the flow was carried out only in steady state conditions; the objective of this study being to describe the mean flow phenomena in order to compare them to the experimental mean shear rates and velocity fields.

3.1 Numerical determination of wall shear rate

In Cartesian coordinate system, the wall shear rates are calculated using the following equations:

$$
\begin{aligned}
S_x &= \left[\frac{\partial v_x}{\partial z}\right] \\
S_y &= \left[\frac{\partial v_y}{\partial z}\right] \\
S_z &= \left[\frac{\partial v_z}{\partial z}\right]
\end{aligned}
\tag{7}
$$

where v_x, v_y and v_z are the velocity components along the spatial coordinates x, y and z, respectively.

The numerical estimation of the wall shear rate is averaged over the entire surface of the microprobes. The calculations are made at the exact location of the electrodes, it allows to analyze the effects of vortex structures on the wall shear rate.

The determination of the 3 components of the wall shear rate (S_x, S_y, S_z) is also performed in order to estimate their respective weight (Fig. 6). Concerning the experimental measurements, they are supposed to correspond only to the axial component, S_y in the mixing channels and, in the same way, to S_x in the inlet channels (Reiss and Hanratty 1963).
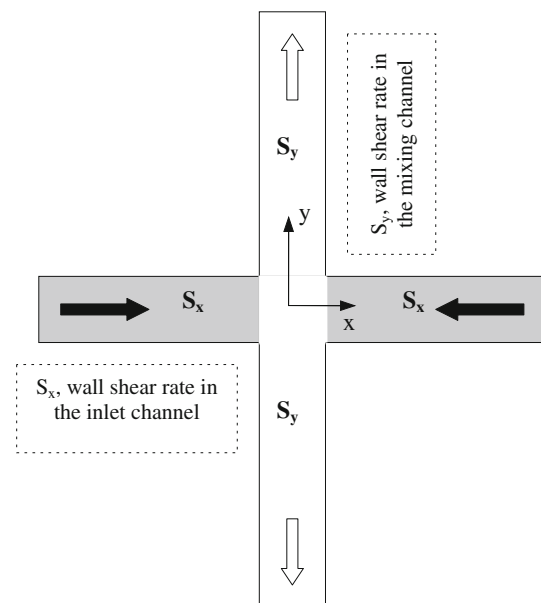

Fig. 6 Distribution of the wall shear rate measured by the electrochemical method. S_x: in the inlet channel and S_y: in the mixing channel

4 PIV characterization of micromixers

A PIV set-up was used for the visualization of the flow behaviour in the T-shaped and cross-shaped micromixers (Fig. 1). The velocity fields are measured for a large range of Reynolds numbers and at different sections of the microchannels. Finally, these experimental results are compared with the CFD study.

Figure 7 shows the velocity fields and velocity profiles V_x measured in the impingement zone flow for a Reynolds number equal to 50. The streamlines are also superimposed to the velocity profiles in Fig. 8, in order to visualize the flow topology.

In Fig. 7, the agreement of the simulation and PIV results is quite good for the profile of velocity vectors and for the stagnation zones shapes. However, in Figs. 7 and 8, the amplitudes of velocities obtained by numerical simulation are higher than those measured by PIV. In the cross-shaped micromixer, we have also observed experimentally that the flow is not symmetrical in each of the inlet and outlet channels and that it is difficult to obtain identical flow rates in the two outlet channels. The average of the scatter between the outlet flow rates is about 6%. This scatter is probably due to the effects of the roughness of the micro-channels and to other experimental imperfections which influence the flow distribution in the outlet channels.
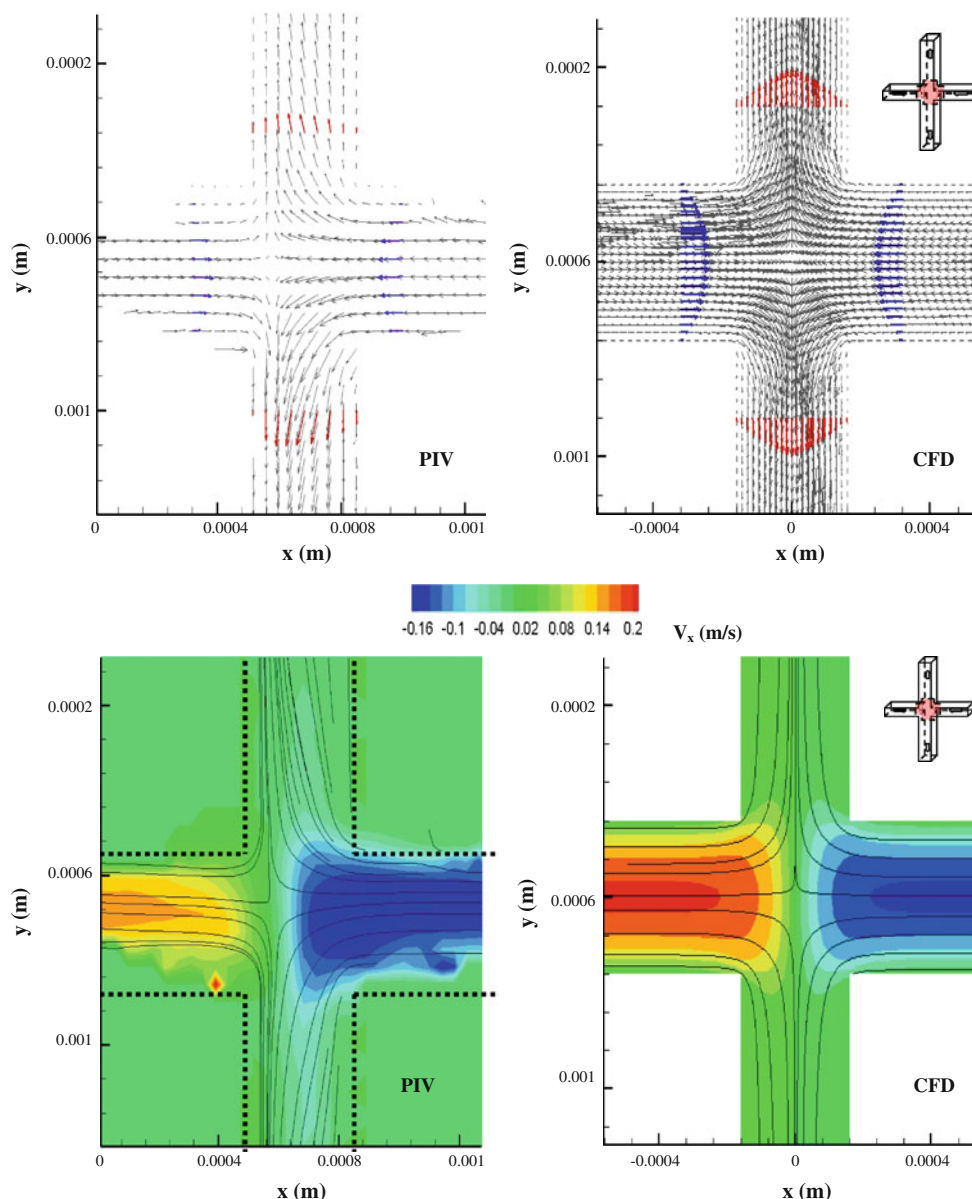

Fig. 7 Velocity fields, streamlines and velocity profiles V_x in cross-shaped micromixer for Re = 50
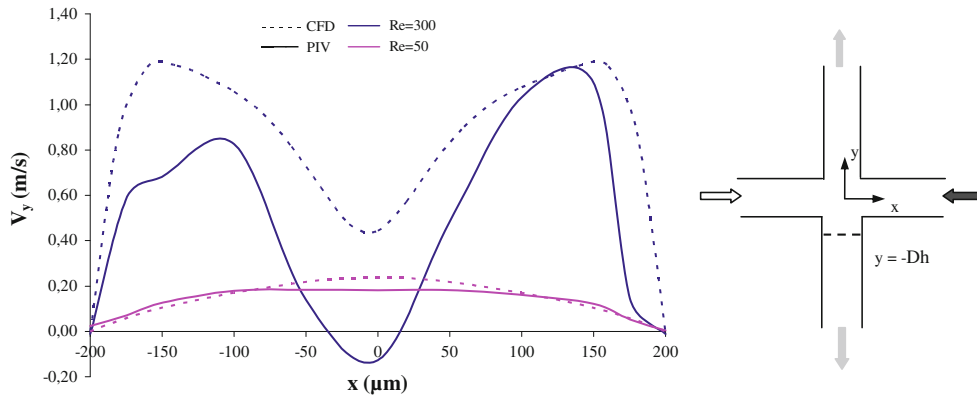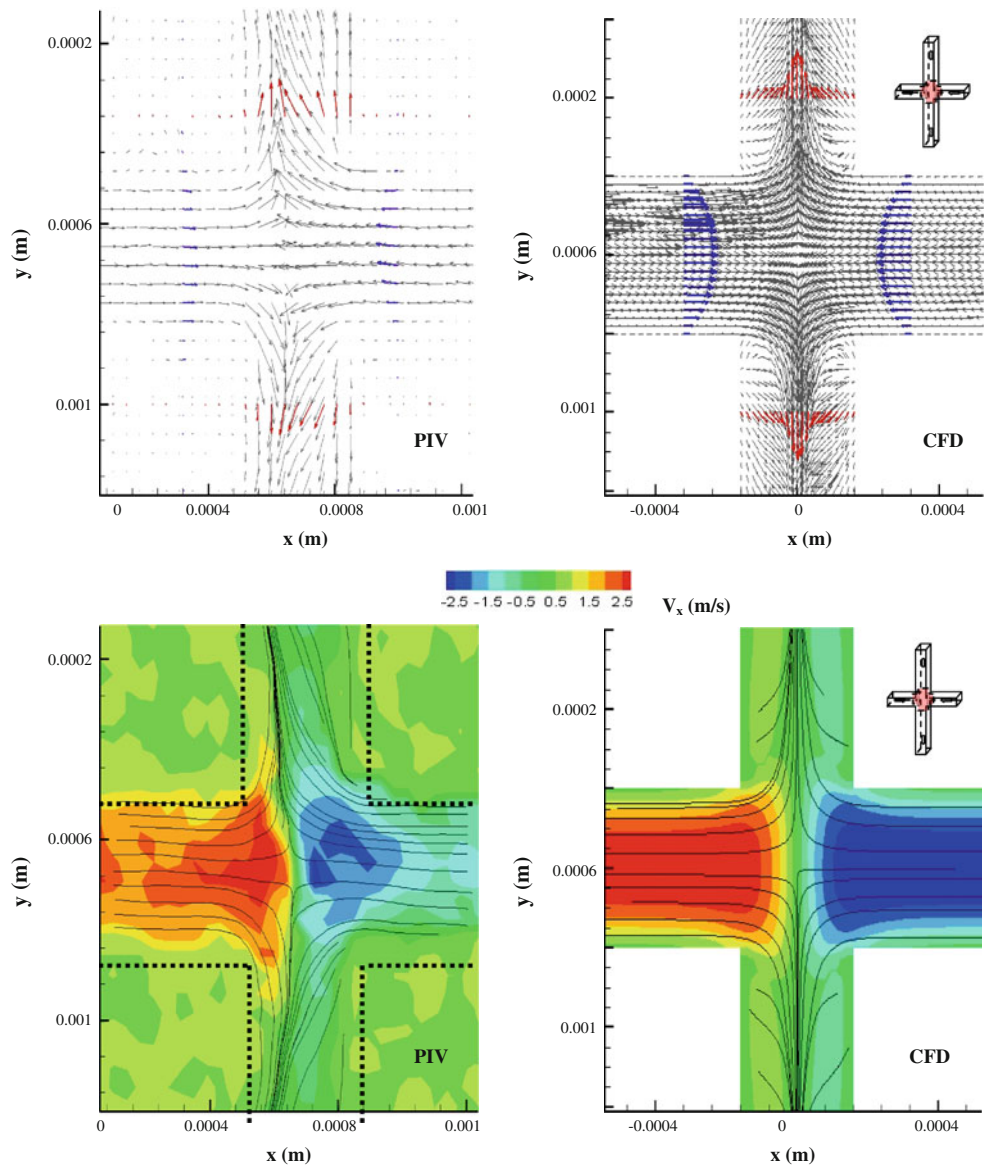
Fig. 8 Velocity profiles in a mixing channel of the cross-shaped micromixer for $y = -D_h$ and $z = 0$

Fig. 9 Velocity fields, streamlines and velocity profiles V_x in cross-shaped micromixer for $Re = 600$

The surface of the channel was observed using an Olympus microscope BX61. The average absolute roughness is not uniform along the microchannels; the maximum value is equal to 0.772 μm.

For Reynolds numbers below 50, the flow does not present a significant area of detachment in both T-shaped and cross-shaped micromixers. After a certain threshold in the impingement zone, the flow divides into two symmetric parts in the direction of the two outlets. The velocity fields remain unidirectional and parallel to the main flow direction (Fig. 7). In Fig. 8, the velocity profile obtained at $z = 0$ and $y = -D_h$ in the inlet of the mixing channel is parabolic and presents a maximum value at the centre of the channel. This flow topology corresponds to the stratified regime (Engler et al. 2004).

For a Reynolds number equal to 600 (Fig. 9), the change of the velocity field direction are observed in the mixing channel compared with the first flow regime (low Reynolds numbers). In the T-shaped micromixer, a recirculation zone, already observed in the numerical study, appears at the top of the impact zone of the fluids. Secondly, from the PIV results, fluctuations in the direction of the velocity fields are observed at the entrance of the mixing channel in

T-shaped and cross-shaped micromixers. The direction of the velocity fields in the mixing channel is not parallel to the mean flow along y direction. On the profile of V_x, the appearance of several blue areas are observed in the mixing channels, corresponding to velocity amplitude equal to 1.6 m s^{-1} for a Reynolds number equal to 600 in the cross-shaped micromixer. With the increase of inlet flow rates, these zones are stretched to a length equal to about 30D_h after the fluids impact. The increasing of the V_x velocity component in the mixing channel corresponds to fluctuations in the direction of velocity vectors and is probably due to the appearance of a three-dimensional flow. The velocity profiles plotted at y equal to $-1D_h$ in Fig. 8 also attest to a change in flow regime.

Finally for the T-shaped micromixer, the evolution of flow patterns and velocity fields corresponds to the experimental results obtained by Hoffmann et al. (2006). But in the literature, the PIV measurements were performed on a plane parallel to the flow, like in Figs. 7 and 9. It makes difficult the visualization of the rotation of the flow in the mixing channel. In order to verify the vortices formation described numerically, we studied the velocity fields in a second measurement plane. The camera is fixed
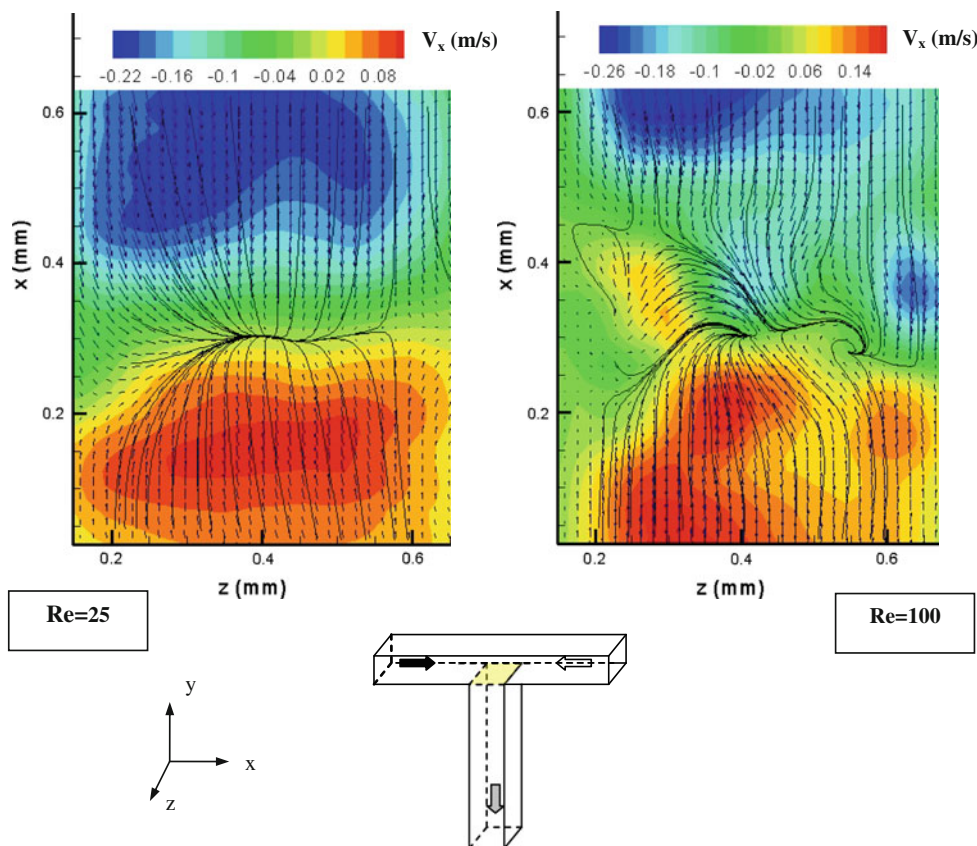

Fig. 10 Velocity fields, streamlines and velocity profiles V_x in T-shaped micromixer for Re = 25 and Re = 100

perpendicularly to the flow direction along y and to the laser plane. Figure 10 illustrates the flow in the inlet of the mixing channel for Reynolds numbers equal to 25 and 100.

In the inlet of the mixing channel, at the position $y = -D_h$ and for a Reynolds number equal to 25, the velocity fields intersect and head toward the outlet (Fig. 10). The directions of velocity fields and streamlines are parallel to the direction of the inlet fluid, which shows that the flow does not present a significant rotation area after the impact zone.

For a Reynolds number equal to 100, the velocity vectors change of direction just after the impact of the fluids. The streamlines in Fig. 10 show that vortex structures are formed. In T-shaped micromixer, PIV measurements in the second plane confirm and illustrate the appearance of a three-dimensional vortex flow for Reynolds numbers greater than 50.

Nevertheless, a quantitative interpretation of the results remains difficult given the limitations of the PIV technique. In PIV measurements made in the second tested plane, the study is limited to Reynolds numbers below 150, because for higher fluid velocity, the reliable acquisition of PIV velocity fields in this plane is no longer technically possible. For this reason, the particles which move in the perpendicular direction to the studied plane can not be captured in successively acquired photos. In the cross-shaped micromixer, the PIV measurements in the second plane are not possible because of optical problems; the acquired PIV images are not clear enough and are too bright.

5 Experimental and numerical wall shear rate results in cross-shaped micromixer

In this section, the comparison between experimental and numerical values of mean wall shear rate is made in different flow regimes. Some experimental and numerical profiles allow to detect the recirculation and acceleration zones as a function of the position of the probes in the cross-shaped micromixer.

Figure 11 illustrates, for a large range of Reynolds numbers, the variations of the mean wall shear rate in impacting flow. Concerning four probes locations S1, S2, S3, and S4, respectively, simulated results are compared with the experimental data obtained using the electrochemical method. The evolution of the experimental mean shear rate with Re tends to be in good agreement with that predicted by the CFD simulations for Reynolds number ranged between 50 and 600. It can be noticed that after the impingement (from the intersection, $y = 0$) the experimental values of the wall shear rate increase with the Reynolds number. The average difference between
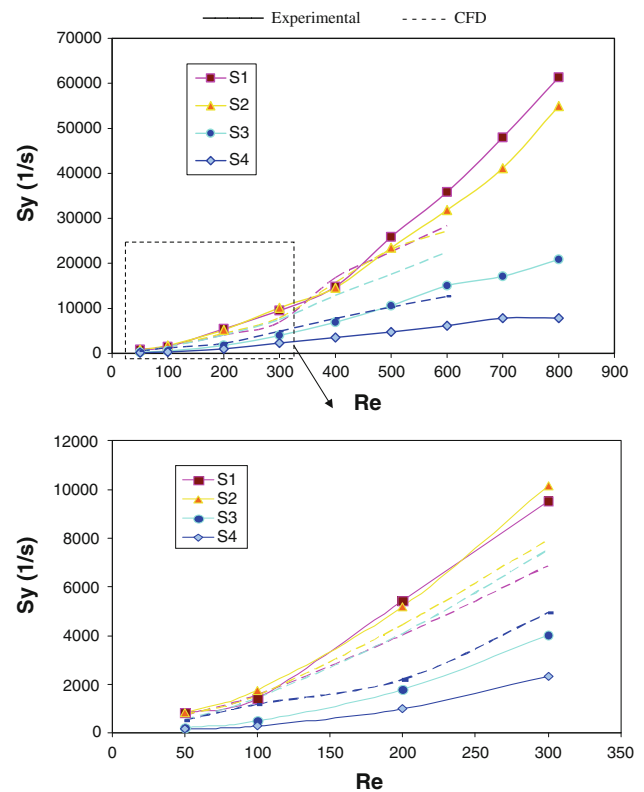

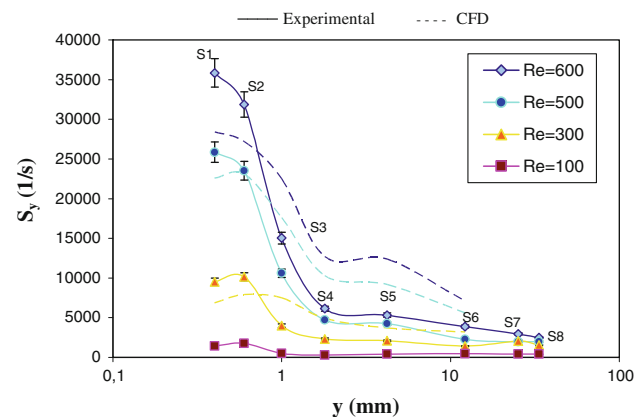Fig. 11 Evolution of the mean shear rate with Reynolds number

Fig. 12 Shear rate profile in the cross-shaped micromixer

numerical and experimental results is ranged between 20 and 50%. The difference between CFD and electrochemical measurements can be partially attributed to the imperfections of micro-current measurement and treatment as well as to the imperfection of the building of the electrochemical cell (size and shape of electrodes, roughness of the channels), which are not taken into account in the numerical approach. Nevertheless, trends are similar between the numerical and experimental data, and then it can be considered that the preliminary simulations provide a good overview of the flow in such micromixers.
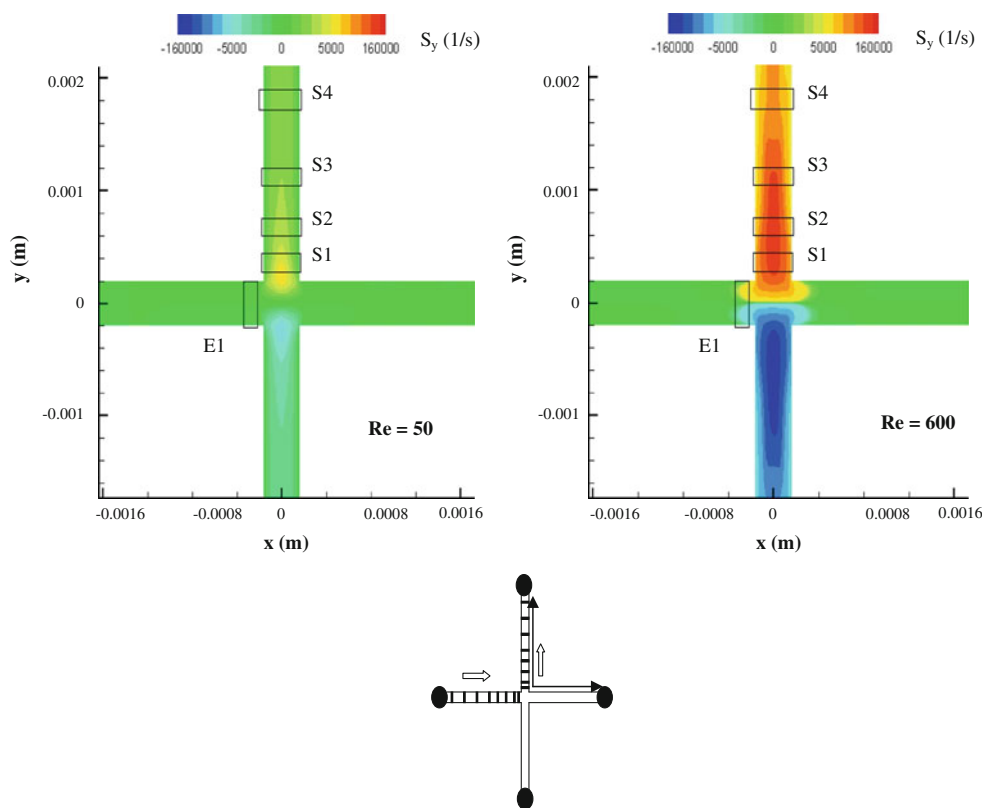
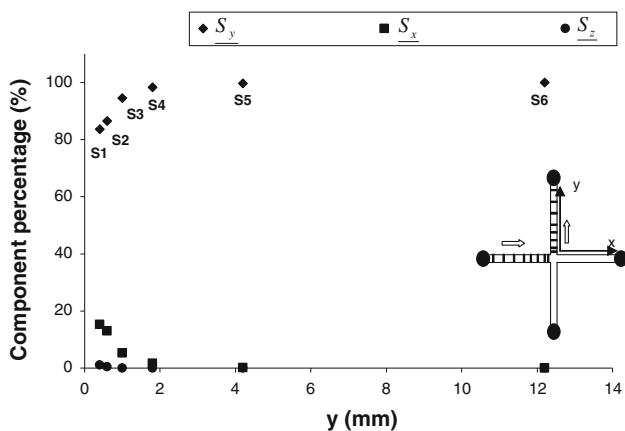**Fig. 13** Wall shear fields in the impact flow for Re = 50 and 600

Fig. 14 Percentage of each component of the wall shear rate calculated on different microprobes for Re = 300

After the fluid impact, Fig. 11 shows that for all positions of the probes, the wall shear stress increases as a function of the Reynolds number. For a Reynolds number lower than 100, the effect of the intersection of the fluids on the shear rate remains negligible. The low values of the wall shear rate are due to a stable flow without vortices structures. But for a Reynolds number varying between 100 and 800, Fig. 11 shows that the flow impact has a significant effect on the increase of the wall shear rate.

Figure 12 presents the profiles of the mean shear rate in the case of the cross-shaped micromixer. From the electrode S6, the values of the shear rate stabilize in the experimental case and it can be noticed that for Re less than 800:

$$Sy1 > Sy2 > Sy3 > Sy4 > Sy5 > Sy_6 \approx Sy_7 \approx Sy_8$$

The wall shear rate measured at positions S1 and S2 are close, it may be explained by the nearness of these two probes. These results are confirmed by the profiles of the wall velocity gradient presented in Fig. 13 for Reynolds numbers equal to 50 and 600.

The higher values measured on probes S1, S2 and S3 in the impact fluid zone can be related to the appearance of a three-dimensional flow observed during the PIV and numerical studies (Fig. 12). Thus, the probes S1, S2 and S3 are located near the zone of vortices formation for a Reynolds number greater than 50 (Fig. 13). The vortex structures interact with the wall boundary layer and induce an increase of wall shear. Till a Reynolds number equal to ∼300 and from the position of the probe S4, the values of wall shear rate are stabilized. Indeed, the vortices decay after the probe S4. For higher Reynolds numbers, the flow becomes unidirectional from the probe S7.

5.1 Numerical components of the wall shear rate

In this paragraph, the effect of vortices on each component of the wall shear rate (S_x, S_y, and S_z) is numerically evaluated at the probe. Figure 14 shows the percentages of each component of the wall shear rate calculated at a probe and determined by the following equations:

$$\underline{S_x} = \frac{S_x^2}{S^2}, \ \underline{S_y} = \frac{S_y^2}{S^2}, \ \underline{S_z} = \frac{S_z^2}{S^2} \tag{8}$$

with: $\underline{S_x} + \underline{S_y} + \underline{S_z} = 100$ (9)

Here, $\underline{S_x}$, $\underline{S_y}$ and $\underline{S_z}$ are percentages of components of the wall shear rate.

In the case of a cross-shaped micromixer, the probes S1 and S2 measure predominantly the axial wall shear rate (S_y); but are also affected by the transverse component (S_x). The electrodes S1 and S2 are located immediately after the fluid impact and are disturbed by the three-dimensional flow structures (Fig. 14). The following probes S3, S4, S5 and S6, respectively, are located in an area without vortices flow; then, the wall shear rate measured on them depends only on the axial component (S_y). The normal component (S_z) of wall shear rate is always negligible (Fig. 14).

Finally, having in mind that the electrochemical measurements are assumed to correspond only to the axial component, S_y (Reiss and Hanratty 1963), we can conclude that the experimental and the numerical wall shear rates can be compared directly, except at the electrodes S1 and S2 for which the numerical wall shear rates are also affected by the transverse component, S_x.

6 Conclusion

In this article, the flow behaviours of the T-shaped and of the cross-shaped micromixers were studied through CFD simulations and experimental investigations. Comparing both micromixers, it is observed from PIV and numerical results that the vortex areas cover a longer part of the mixing channel in the case of the cross geometry. A maximum distance of three-dimensional flow equals to $7D_h$ is observed in the T-shaped micromixer, whereas the vortices are observed until a length equal to approximately $25D_h$ in the cross-shaped micromixer. In comparison with the cross-shaped configuration, the effect of microchannels confinement and the degree of freedom for the flow are lower in the T geometry. It induces the rapid disappearance of vortices and inhibits the flow rotation in the mixing channel. Considering identical inlet flow rates, it may be expected that the highly three-dimensional behaviour of the flow in the cross-shaped micromixer could improve the

mass transfer between the fluids by convection in the mixing channels, compared to the T-shaped geometry.

In the cross-shaped micromixer, the experimental measurements of mean wall shear rate from various microprobes flush-mounted to the wall, allow to emphasize several points. A certain difference exists between the numerical and experimental results; this can be partly attributed to the imperfections of the building of the electrochemical cell, such as the real size, shape and roughness of the electrodes, the roughness of the channels, and partly due to experimental uncertainties involved during the implementation of the electrochemical method. Nevertheless, concerning the evolutions of the values of the wall shear rate versus Re, similar trends are observed in experimental and numerical results. Moreover, the scatters between experimental and numerical data are ranged between 20 and 50%, which remain satisfying because the order of magnitude is confirmed. Secondly, the high values of wall shear rate, in the impact zone, confirm the near wall disturbance created by the impingement of the flow and also the appearance of vortices.

In a next step of our study, the quantifying of the mixing between species will be estimated by numerical calculations and experimentations performed by Confocal Laser Scanning Microscopy (CLSM) in both T and cross geometries.

References

Ait Mouheb N, Solliec C, Montillet A, Comiti J, Legentilhomme P, Havlica J (2008) Numerical study of the flow and mass transfer in micromixers. In: ASME Conference Proceedings, ICNMM 2008-62273, pp 241–248

Engler M, Kockmann N, Kiefer T, Woias P (2004) Numerical and experimental investigations on liquid mixing in static micromixers. Chem Eng Sci 101:315–322

Hanratty TJ, Campbell JA (1983) Measurement of wall shear stress. In: Goldstein J (ed) Fluid mechanics measurements. Hemisphere Publishing Corporation, Washington, pp 559–615

Hessel V, Hardt S, Löwe H, Schönfeld F (2003) Laminar mixing in different interdigital micromixers. I. Experimental characterization, AICHE J 49(3):566–577

Hoffmann M, Schlüter M, Räbiger N (2006) Experimental investigation of liquid-liquid mixing in T-shaped micro-mixers using μ-LIF and μ-PIV. Chem Eng Sci 61:2968–2976

Huchet F, Havlica J, Legentilhomme P, Montillet A, Comiti J, Tihon J (2008) Use of electrochemical microsensors for hydrodynamics study in crossing microchannels. Microfluid Nanofuid 5:55–64

Kockmann N (2008) Transport phenomena in micro process engineering. Springer ISSN1860-4856

Lévêque MA (1928) Les lois de la transmission de la chaleur par convection. Ann Mines Paris 13:201–239

Levich VG (1962) Physicochemical hydrodynamics. Prentice Hall, Englewood Cliffs

Mansur EA, Ye M, Wang Y, Dai Y (2008) A state-of-the-art review of mixing in microfluidic mixers. Chin J Chem Eng 16:503–516

Mitchell JE, Hanratty TJ (1966) A study of turbulence at a wall using an electrochemical wall shear stress method. J Fluid Mech 26:199–221

Reiss LP, Hanratty TJ (1963) An experimental study of the unsteady nature of the viscous sublayer. AICHE J 8:54–160

Schrott W, Svoboda M, Slouka Z, Šnita D (2009) Metal electrodes in plastic microfluidic systems. Microelectron Eng J 86:1340–1342

Soleymani A, Kolehmainen E, Turunen I (2008) Numerical and experimental investigations of liquid mixing in T-type micro-mixers. Chem Eng J 135:219–228

Srisamran C, Devahastin S (2006) Numerical simulation of flow and mixing behaviour of impinging streams of shear-thinning fluids. Chem Eng Sci 61:4884–4892

Wong SH, Ward M, Wharton CW (2004) Micro-T mixer as a rapid mixing micromixer. Sens Actuators B 100:359–379